Transparent Electrode with a Nanostructured Coating

Yan Y. Huang* **and Eugene M. Terentjev**

Cavendish Laboratory, University of Cambridge, U.K.

ABSTRACT Using single-walled nanotubes as an example, we fabricated transparent conductive coatings and demonstrated a new technique of centrifuge coating as a potential low-waste, solution-based batch process for the fabrication of nanostructured coatings. A theoretical model is developed to account for the sheet resistance exhibited by layered random-network coatings such as nanofilaments and graphene. The model equation is analytical and compact, and allows the correlation of very different scaling regimes reported in the literature to the underlying coating microstructure. Finally, we also show a refined experimental setup to systematically measure the curvature-dependent sheet resistance.

KEYWORDS: conductivity · graphene · nanotube · nanowire · scaling · deformation

Transparent conducting electrodes, as a key element of the next generation of optoelectronic devices, are entering a new phase of development driven by the growing demands in flexible and compliant electronics.[1−3] Traditional doped oxide thin-film coatings, most notably, indium−tin oxide (ITO), become less attractive due to their limited availability, mechanical rigidity, and high-temperature, high-vacuum processing conditions. Development in nanostructured materials, such as carbon nanotube[4] and graphene,[5] has offered new ways for the realization of flexible transparent electrodes.[6−9] Recent highlights include the roll-to-roll fabrication of a layered-graphene electrode[10] achieving an optical-electrical characteristic superior to that of ITO. In addition to the dry, roll-to-roll process which is only economical for an industrial-scale production, the more widely adapted technique is based on solution-phase deposition. It holds central importance in the fundamental research and development of flexible conductive electrodes, since it allows a versatile selection of source nanomaterials (with a variety of surface modifications) as well as elastic substrates. Once the coatings are deposited, their performances are usually gauged by the sheet resistance (R^s) *vs* optical transmission (T), and the electromechanical response. For these nanostructured coatings, various results (*e.g.*, nanofilament[11−14] and graphene[15−18]) have demonstrated a nonlinear power-law correlation between the sheet resistance and the coating thickness (H), making them distinct from the conventional conductive coatings produced by continuous uniform thin films where $R^s \propto 1/H$. This calls for a new theoretical model which reflects the role played by the microstructures of this type of coatings. Moreover, studies so far also lack a systematic and accurate method to test the change in sheet resistance with respect to electrode deformation/bending. The above two challenges form the main focus of our present study. We employ a solution-based, centrifuge coating technique to fabricate transparent conductive coatings on flexible substrates, using single-walled nanotubes (SWNTs) as a testing system. Through evaluating the interdependence between the sheet resistance and the transparency of our coating, together with a range of data available in literature, a generic theoretical model is proposed which provides good fitting to the behavior observed in both nanofilament (*e.g.*, SWNTs and metallic nanowires) and graphene-based transparent coatings. We show that the commonly observed "power-law" response is a signature of a particular coating microstructure. Finally, we refined a testing geometry which allows accurate determination of the strain-dependent electrical resistance of flexible electrodes.

RESULTS AND DISCUSSION

Centrifuge Coating. A number of solution-based techniques are present in literature[14,19−23] for the fabrication of transparent electrodes with nanoparticulate coatings. Controlling the dispersion state of nanoparticles in solutions is a challenging task due to the significant surface energy and van der Waals attraction acting at the nanometer length scale. To obtain a coating

* Address correspondence to yysh2@cam.ac.uk.

Received for review November 30, 2010 and accepted February 18, 2011.

Published online March 03, 2011
10.1021/nn1033373

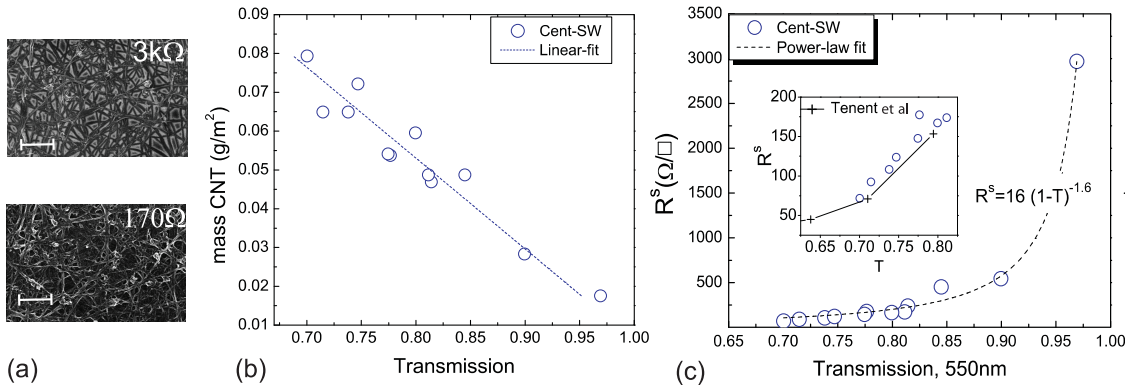

Figure 1. (a) Scanning electron micrographs of two PET films coated with low and high densities of PhrC-SW networks, with the respective sheet resistance also indicated. Scale bar = 500 nm. (b) The total mass of SWNTs added for coating plotted against the resulting coating transmission (at 550 nm); the result also confirm the linearity in the low-absorption regime. (c) Plot of sheet resistance against transmission (at 550 nm) for the centrifuge-coated SWNT networks (acid treated). An approximate power-law dependence is observed. Insert compares our coating performance with that produced from an ultrasonic spraying technique.[23]

of well-dispersed, uniformly distributed nanoparticles, fabrication processes would require either to "quench" the temporarily dispersed state, or to use dispersion agents followed by centrifugation to eliminate the clusters, leaving a relatively stable solution prior to coating deposition. Vacuum filtration[6,22] and spray deposition,[14,23] being two of the most common solution processing methods, operate on the basis of these principles, respectively. However, their applications were limited by either the deposition area or the large amount of nanoparticle waste generated. Centrifuge coating, by comparison, enables the fixation of a metastable dispersion of nanoparticles onto large areas of substrate films. Its operating principle is schematically shown in the Supporting Information Figure SI(1), where a solution placed in the cylindrical container is forced to spread onto the side-wall under the centrifugal force. When the centrifugal acceleration (a_c) much exceeds the gravitational acceleration (g), the solution surface becomes close to parallel to that of the vertical sidewall. For instance, at a mild spinning rate of $a_c = 57g$, the fluid surface only deviates from vertical by 1°; in our preparation, we used approximately twice that rate. The thickness H of the resulting coating is thus controlled by the total solute input and the area of the"side-wall" to be coated. The rate of evaporation can be controlled by the evaporation channels in the centrifuge reactor lid, as well as the external heating supplied. Therefore, temporarily dispersed nanoparticles can be fixed at the target substrate by simultaneous effects of the particles being pushed to the substrate, and the fast evaporation of solvent.

We employed this technique to coat SWNTs on polyethylene terephthalate (PET) substrate followed by acid treatment to remove the PhrC-surfactant. The detailed fabrication procedure is described in the Methods section. The SWNT-PET electrodes produced from our centrifuge coating geometry were 1.5 cm wide and 18 cm long, the size of which is only limited by the dimension of the evaporation container. Scanning electron micrographs of two PET films, coated with low and high densities of SWNT networks, are as illustrated in Figure 1a. Centrifuge coating offers a controlled evaporation process, which means that both high and low boiling point solvents can be used, facilitating direct deposition of coatings onto different surfaces when compatible solvents are chosen. Using an SDS-stabilized SWNT solution, we also fabricated coatings onto the acrylic and PDMS elastomers (nonacid treated), Table c in Supporting Information, SI(2). Benefiting from the low-waste coating process, only a small quantity of starting materials is required for a particular optical transmission, Figure 1b. This enhances the control and reproducibility of the film since the exact amount of SWNT input is known, rather than being based on estimations from additional solution absorption measurements after the cluster separation experiments. The sheet resistance−transmission performance of our SWNT electrodes, illustrated in Figure 1c, is comparable to that of Tenent *et al.*,[23] an acid treated SWNT coating fabricated by ultrasonic spraying. We found that the dependence of R^s on T can be well fitted to a power law relationship:

$$R^s = R^*(1 - T)^{-\gamma} \quad (1)$$

Correlating the Microstructure and Conductivity Performance. In general, the transmission of light through a medium of thickness H can be described by the Beer−Lambert law, $T = I/I_o = \exp(-H/\bar{H})$, with I_o and I being the initial and final light intensity, respectively, and $\bar{H}$ being the penetration depth characteristic of the medium. $\bar{H}$ is approximately constant for films produced by the same nanomaterials and fabrication procedure. Graphene and SWNT coatings of different thicknesses

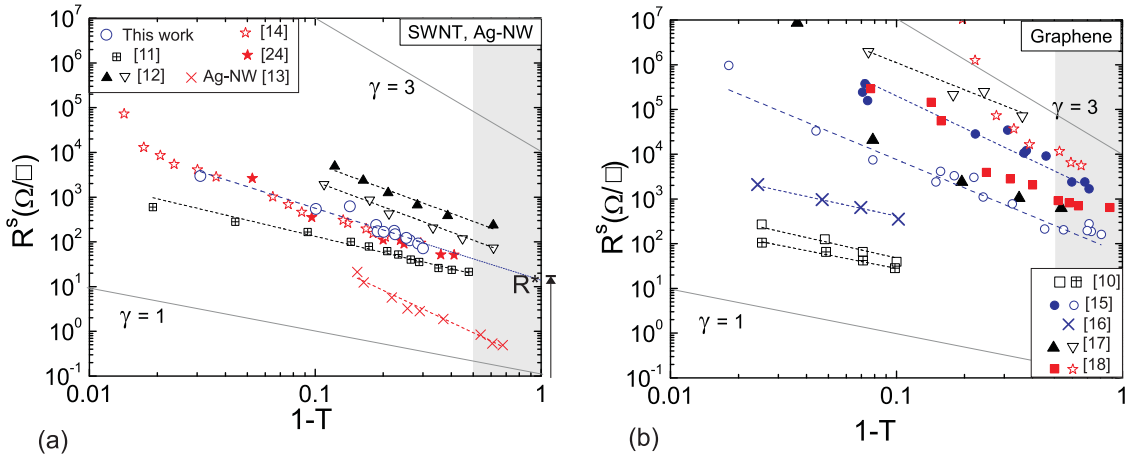

Figure 2. Log−log plots of sheet resistance R^s against coating absorption $(1 - T)$ for conductive nanostructured coatings produced by (a) nanofilaments and (b) graphene. Intercept at $T = 0$ gives the value of R^* for eq 1. The shaded areas indicate the coatings entering the less transparent region with $T < 0.5$.

were also found to follow this relationship (see data fitting in Supporting Information, Figure SI(3) and also ref 25). At high transmission, the regime within which the transparent electrode ideally operates, the equation is reduced to $T = 1 - H/\bar{H}$ or $1 - T = H/\bar{H}$. Rearranging eq 1, one obtains $R^s = R^*(H/\bar{H})^{-\gamma}$. For a continuous conducting thin film $\gamma = 1$, that is, R^s is inversely proportional to H, a classical Ohmic dependence. However, our data apparently deviates from such a standard result. To validate whether this is a special case and investigate the reasoning behind, we further analyzed the R^s *vs* T data of different conductive nanostructured films from the literature, summarizing the data in Figure 2.

Although vastly different fabrication methods are adapted for the deposition of nanofibers and flakes, they all have one feature in common: being a layer-by-layer process. Figure 2a summarizes the electrical-optical correlation of a range of nanofilament coatings: SWNTs (grown by CO disproportionation[12] and arc-discharge[11,14,24]), double-walled carbon nanotube,[12] and silver nanowires,[13] each of which is fabricated through a different method and/or postcoating doping. Strikingly, they all seem to show some degree of power-law dependence as indicated by the linearity of a log−log R^s *vs* $(1 - T)$ plot. It is clear that the exponent γ varies across many systems and does not take a value of 1 as should be in the classical Ohmic resistance. The same analysis was also carried out for the graphene coatings (as-grown[10,16] or exfoliated[18] graphene; and solution processed reduced graphene oxide[15,17]), where most of them also follow the same trend except those of ref 18 which deviate toward the high transmission region (low values of $(1 - T)$). Extrapolation of the log−log plot to $(1 - T) = 1$ gives the prefactor R^* in the power law of eq 1. The exponent and prefactor fitted for each data set, along with the brief description of the coating types, can be found in the Supporting Information, Table 1.

The pioneering studies by Hu *et al.*[22] on SWNT network electrodes suggested the correlation between transmission (in the visible spectra) and sheet resistance R^s should follow a metallic skin-effect model for electromagnetic waves[26] expressed by:

$$T = \frac{1}{\left(1+\frac{2\pi}{c}\sigma_{ac}H\right)^2} = \frac{1}{\left(1+\frac{2\pi}{cR^s}\frac{\sigma_{ac}}{\sigma_{dc}}\right)^2} \quad (2)$$

where $R^s = 1/(\sigma_{dc}H)$, and c is the speed of light.

This leads to a figure of merit, the ratio between DC to optical-frequency conductivity σ_{dc}/σ_{ac} for the transparent coating, which has subsequently been adapted by other studies[13,24] as the standard to compare their coating performance. It is noted that the above model only holds for a continuum conducting medium having a refractive index invariant of thickness. Systems with optical properties satisfying this relationship should follow a scaling slope of −1 in the log−log plot of R^s *vs* $(T^{-0.5} - 1)$. However, most of the nanofilament and graphene coatings do not comply with the above criteria, see Supporting Information, Figure SI(4).This calls for an alternative model to better reflect the underlying network microstructure and the charge transport mechanism in thin nanoparticulate coatings.

The Constrained Random Walk Model. We first set up a model system, schematically illustrated in Figure 3,i−iii, with the objective to evaluate the film resistance perpendicular to its thickness (z-axis), that is, along the length direction (y-axis). Let us assume that, due to the nature of deposition process, the morphology of the film is homogeneous along the plane, and the width (W) and length (L) of the film are large. One can imagine the film to be formed by pseudolayers of conducting planes, on which electrons can travel freely in the y-direction under an applied electric field. The total resistance is determined by the resistance of the film per unit width, and hence we only need to consider the electron transport

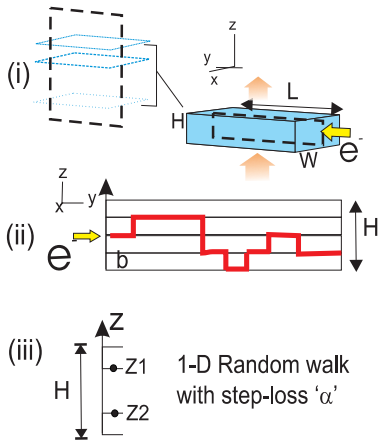

Figure 3. Overall scheme of the "constrained random walk model": (*i*) pseudoconduction planes for the drifting electrons; (*ii*) a probable flow path for an electron drifting along the *z*-axis when encountering "obstacles"; (*iii*) the final 1-D random walk model which was employed in our calculation.

along the *y*-direction in a selected *y*−*z* plane, Figure 3ii. On the other hand, electrons are also allowed to jump across to a neighboring layer along the *z*-axis, the probability of which can be assumed to be Gaussian (*i.e.*, that each jump is associated with an energy barrier E_j). We can simplify the problem to a 1-D random walk along the *z*-axis, for any arbitrary starting position z_1 and ending position z_2. All steps of such a walk are confined by *H*, the thickness of the coating. A path can take *N* steps up and down, but each step is associated with a finite reduction in conductance, expressed by a *relative* factor α (α ≥ 1), which is a function of E_j. Our aim is to determine the total amount of conduction (C_z) along the *z*-axis within the spacing *H*. This is determined by the probability of a conducting path Ω (constructed by all the possible *N*-number of steps), factored for the conductance loss on each z-jump:

$$C_z = c_0 H \Omega \left(\frac{1}{\alpha}\right)^N \quad (3)$$

where c_0H is the bare conductance of an average path and the probability Ω is given by the classical problem of a random walk between two walls:[27]

$$\Omega = \int_0^\infty dN \frac{2}{H^2} \int_0^H dz_1 \int_0^H dz_2 \sum_{p=1}^{\infty} \sin\frac{p\pi z_1}{H} \sin\frac{p\pi z_2}{H} \exp\left(\frac{-p^2\pi^2 N b^2}{6L^2}\right)$$

where *b* is the step length of random walk. The solution to the above yields:

$$C_z = c_0 H \left[1 - \frac{1}{2\sqrt{\ln\alpha}\,\frac{H}{b}} \tanh\left(2\sqrt{\ln\alpha}\,\frac{H}{b}\right)\right] \quad (4)$$

From the above expression, we clearly see the dependence of C_z on *H*, the thickness of the coating. When $H \gg b/(\ln\alpha)^{1/2}$, eq 4 is simply reduced to $C_z = c_0H$. This corresponds to the bulk behavior, a classical Ohmic case, where the conductance is linearly scaled with cross-sectional thickness (or resistance is inversely proportional to cross-sectional thickness). On the other hand, how does the *relative* cross-layer reduction factor α affect the dependence of C_z−*H* for intermediate values of *H*? Two limiting cases are considered here. First when α is close to 1, the conducting path is jumping between layers and therefore it has a high roughness. In this case we have $C_z/c_0 = \pi^2(H^3/12b^2)\ln\alpha$, which predicts the resistance ($R \propto 1/C_z$) to depend on H^{-3}. On the other hand, when $\alpha \gg 1$, the *z*-jumps of the conducting path are not favorable and the charge carriers move more or less within plane layers. In this case we again obtain $C_z = c_0H$; that is, the total conductance is simply a sum from each flat path. Before we investigate the physical meaning of the various parameters and scaling regimes, let us first assess whether the proposed model agrees with the experimental data. To do this, we uses an alternative representation of eq 4 as,

$$\frac{C_z}{c_0 b} = \frac{H}{b}\left[1 - \frac{1}{2\sqrt{\ln\alpha}\,\frac{H}{b}} \tanh\left(2\sqrt{\ln\alpha}\,\frac{H}{b}\right)\right] \quad (5)$$

C_z/c_0b can be seen as a nondimensional parameter arising from the probable electronic diffusion along the thickness direction. The inverse of this parameter, c_0b/C_z quantifies the resistance along the coating thickness. c_0b/C_z is plotted against H/b for selected values of α in Figure 4a,b. For the experimental results, their reduced sheet resistance R^s/R^* is plotted against $(1 - T)$, which is directly proportional to coating thickness for reasonable coating transparency. Therefore, the "scaling" between R^s/R^* and $(1 - T)$ also reflects a similar dependence between R^s/R^* and the coating thickness. Comparing the theoretical and experimental results, one finds a high degree of matching for the various nanofilament coatings. In particular, we expect in this case the step length *b* to be of the order of filament (*e.g.*, nanotube) diameter, and indeed the thinnest coating of the data set[24] is at $H \approx b$, that is, practically a monolayer of CNTs. For the graphene coatings, an exception appears to be for the data from ref 18, such that the sheet resistance was reduced more sharply than prediction for the initial deposition of their thinnest coating (*i.e.*, for $(1 - T) < 0.25$). Nevertheless, the subsequent data also follow the predicted trend. It is also interesting to note that the effective *z*-step length of a conducting path *b* is also close to the thickness of graphene layer, as the lowest H/b points of refs 10 and 16 indicate. On the basis of the above analysis, we would like to conclude that the

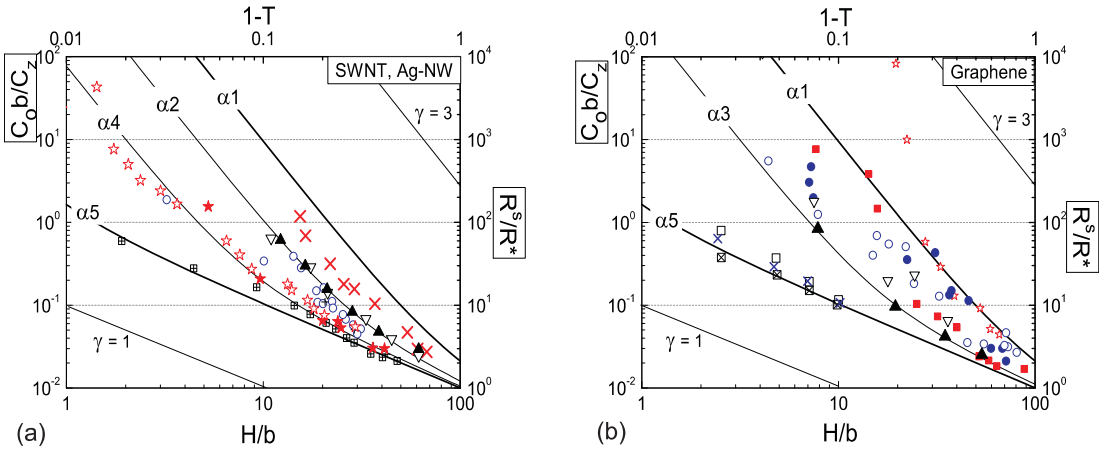

Figure 4. Comparison between the modeled data, $(c_0b)/C_z$ *vs* H/b, and experimental data, R^s/R^* *vs* $(1 - T)$, for various nanofilament (a) and graphene (b) coatings. Here, $\alpha_1 = 1.00008$, $\alpha_2 = 1.0008$, $\alpha_3 = 1.0025$, $\alpha_4 = 1.1$, $\alpha_5 = 5$. The labels for the experimental data are the same as those shown in Figure 2 panels a and b.

commonly asserted $R^s = R^*(1 - T)^{-\gamma}$ scaling behavior with the exponent range $\gamma \approx 1-3$ is due to the transition from a thin-film to a bulk structure of a multilayered network. The exact form of correlation is significantly affected by the magnitude of α, the measure of the barrier for charge carriers to transverse the layers. Using different real systems as examples, we will discuss how the model can reveal the associated coating microstructure.

A relatively high magnitude of α indicates the preference of electrons to drift parallel to the applied electric field without diversion to neighboring layers, leading to an overall exponent γ close to 1. For this to take place, there should be a good continuity of conduction path bridging the start and the end probes. From Figure 4b, one may note that one to few-layers of flat, well-stacked graphene sheets, such as those fabricated by ref 10 and ref 16 using direct transfer of as-grown graphene to a flexible substrate, demonstrate exactly this behavior. In contrast, solution deposition of exfoliated graphene (or graphene oxide) tend to have smaller α values and larger resulting apparent exponent ($\gamma > 2$), which is in accordance with the random stacking, greater roughness of conducting paths produced by these processes. Although most SWNT coatings were produced by solution deposition, their large lengths assist the in-plane transport of electrons (bearing in mind that most tubes are preferentially laid flat to the substrate); as a result, their exponents are all shown to lie below 2 (*cf.* Figure 2a). For coatings formed by nanofilaments, the length of the fiber is a key parameter controlling the thickness-dependent behavior: once in a fiber, an electron can flow relatively freely until it reaches the end of the fiber. Data from silver nanowires (Ag-NWs) act as a good comparison to the results from SWNTs in Figure 2a and Figure 4a. Having a much smaller aspect ratio (fiber diameter, ~80 nm; length, ~6.5 μm) than SWNTs, Ag-NWs show a much stronger dependence of R^s on the coating thickness; that is, the electrons are having to jump across layers making very rough paths. Accordingly, our theory also predicts that a nonunit exponent γ would always exist for nanofilament coatings because of the finite filament lengths.

Electromechanical Performance. In addition to good optical-electrical properties, a transparent flexible electrode should also have suitable electromechanical characteristics. For a coating which is firmly attached to the surface of the bent substrate, a strain is induced in the coating which is inversely proportional to the radius of curvature. Precise control of the radius of curvature imposed on the film is critical to measuring the change in coating resistance upon deformation. Most of the current measurement techniques are based on free bending of an electrode film forming a circular shape;[10,24] the radius of curvature is often poorly defined and may be inhomogeneous because not the whole film could experience the same curvature, and the proportion of film undergoing the actual deformation also changed throughout the changing of bending application. To refine the testing, we examine the static bending resilience of our electrode by confronting the PET backing against cylinders of known radius r, Figure 5a. In each bend test, we ensure that the length of the electrode covers more than half of the circumference of the cylinder. When the coated side of PET is facing outward, the coating is subjected to a tensile strain, which is evenly distributed cross the full length of the film. Subsequently, two parallel electrodes are brought in contact with the coating at the tangential points of the circularly bent film. In this way, the resistance, denoted as R_r is always measured for a length of a half circle (πr). Separately, we perform 2-probe resistance measurements (R_L) on flat coatings with different probe spacings. A commercial ITO coated-PET film (Sigma Aldrich, with ITO thickness 75 nm, quoted

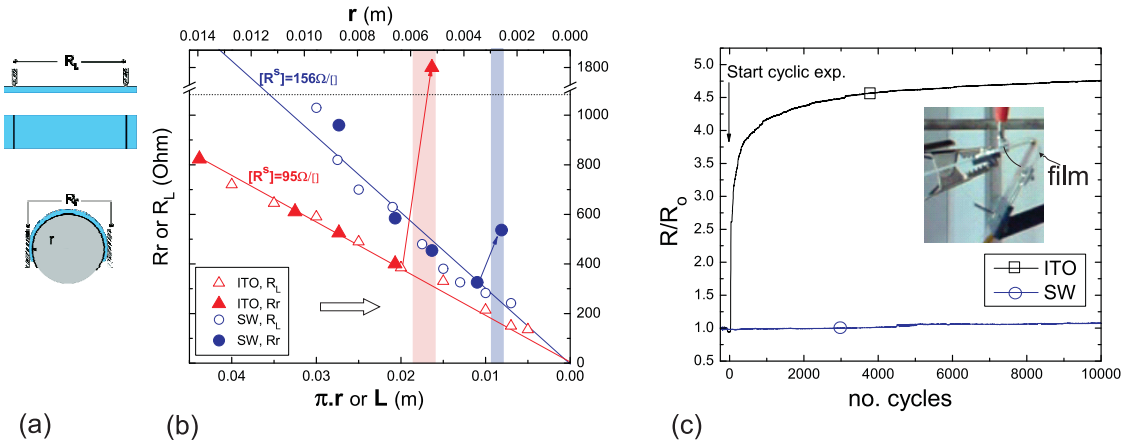

Figure 5. (a) Scheme showing the experimental setup for the determination of static electromechanical performance of a flexible electrode. (b) Plot of in-plane resistance against the probe spacing for SWNT- and ITO-coated PET films. The shaded regions indicate the radius of curvature at which bending starts to affect the integrity of the coating. (c) Plot of variation in the sheet resistance R/R_o against the number of bending cycles for SWNT and ITO coatings, with the insert showing the experimental setup.

sheet resistance $R^s = 70-100\ \Omega/m^2$) is also tested as a reference.

Figure 5b shows the change in coating resistance *versus* the effective probing spacing, L or πr, depending on geometry. When the films are unbent, both coatings yield a linear dependence of resistance R_L on the probing distance, a behavior expected by materials with uniform in-plane sheet resistance. If we define $R = \rho L/(WH)$, with W and H being the width and thickness of the coating, the slope of the $R-L$ plot is equal to $\rho/(WH)$. The sheet resistance, $R^s = \rho/H$, thus can be determined from the slope of the $R-L$ plot, and the width of the coating. This gives 156 and 95 Ω/m^2 for the selected SWNT and ITO coatings, respectively. They both agree reasonably well with the average sheet resistances obtained by a 4-probe method, which are 160 and 92 Ω/m^2, respectively. Plotting the $R_r-\pi r$ data on the same plot, one noticed that initially for large radii of curvature, R_r follows the same trend as R_L. In other words, the tensile strain imposed on the coating has negligibly damaged the coating. At a radius of curvature just above 5 mm, the ITO coating underwent a sudden increase in resistance to 6 times its undeformed value (for the same length of coating). Taking the geometry of the PET backing film into account, the radius of curvature for the onset of damage would correspond to a tensile strain $\varepsilon \approx 0.01$ in the ITO. This is slightly lower than but comparable to the critical $\varepsilon \approx 0.02$ reported for a 105 nm ITO coating on PET tested by uniaxial tensile elongation.[28] The sheet resistance of SWNT-coating, on the other hand, was not affected by bending for $r > 2.5$ mm ($\varepsilon < 0.02$). At the threshold $r \approx 2.5$ mm, one sees a 50% increase in resistance due to the coating damage, of which the magnitude is appreciably smaller than that of ITO.

Cyclic bending was performed, in a different experimental setup, by fixing a constant length of coating between two electrodes and varying the folding angle ϕ between 55° and 30°, Figure 5b insert. Although the proportion of the film being bent is varied with ϕ due to the rigidity of the PET backing layer, such a testing condition gives a good simulation to the ordinary cyclic deformation that a flexible display would experience. By using the same dimension of coated PET for both SWNT and ITO, the performance between the two can be compared. The change in coating resistance R/R_o (R_o being the initial resistance of the undeformed coating) is monitored for 10^4 cycles at a deformation rate of 2 cycles/s. It was found that ITO coating underwent resistance increase during the first hundreds of cycles after which the value became stable. On the other hand, no noticeable change in film resistance was observed for the SWNT coating.

CONCLUSION

We have demonstrated the feasibility of using centrifuge coating as an alternative low waste, large-area solution processing technique for the fabrication of nanostructured coatings. Investigation of various nanostructured coatings has revealed a very different sheet resistance−transmission $R^s = R^*(1 - T)^{-\gamma}$ correlation which cannot be described by the classical thin-film model, making them a special category of conductive coating. The theoretical model is based on counting the random paths of charge carriers through a multiply connected system, which allows a relation between what the broad literature perceives as the "exponent" γ and the optical-electrical behavior of the coatings. The general equation allows the prediction of the system parameters for ultimate coating performance. Electromechanical testing shows that a carbon nanotube network was able to out-perform ITO for both static and dynamic bending resilience. However, a static tensile strain of 2% seems to be too small to cause a bulk 50% change in the resistance by breaking

the semiflexible filaments forming the network. Instead, the external strain causes the reversible disconnection of network junctions. It is hoped that our findings presented here will further the understanding and development of flexible transparent electrodes based on nanostructured coatings.

METHODS

Centrifuge Coating. SWNTs were purchased from Carbon Solutions, Inc., under the P2-SWNT grade (grown by arc discharge process, carbonaceous purity of 70−90%, low functionality, and low chemical doping). Coating was performed on three backing substrates, PET (polyethylene terephthalate), acrylic elastomer, and PDMS (polydimethylsiloxane) elastomer. PET (0.1 mm, biaxially oriented) was purchased from Goodfellow; acrylic form tape was purchased from tapes-direct.co.uk, under the Hi-Bond tape (0.25 mm thick) category. PDMS stripes (0.2 mm thick) were fabricated in-house using the two-part Dow Corning SYLGARD 184 silicone elastomer kit. A different dispersion procedure was adapted for the coating of PET and the other two elastomers.

For the coating of PET, chloroform is selected as a solvent due to its low boiling point such that the process can be carried out at room temperature without external heating. SWNTs were dispersed in chloroform by ultrasonication (Cole Parmer 750 W, titanium microtip) for 5 min after which a fixed volume of solution (5 mL for our container geometry) was fed into the centrifuge coater. At low concentrations (typically 0.01 mg/mL), homogeneous coatings can be obtained without a dispersant; at higher concentrations, a porphyrin−alkane surfactant (PhrC).[29,30] synthesized in-house was used. All the resulting SWNT-solutions can remain visually stable for more than 1 h before sedimentation appears; hence no preliminary filtration or centrifugation was required prior to coating. Centrifuge coating was performed at room temperature, at a rotational speed of 5000 rpm (a_c = 91 g) for 30 min. The coated PET films were then rinsed in chloroform, followed by nitric acid treatment for 30 min and then repeatedly rinsed in distilled water. It is found that acid treatment (labeled "AT") induced insignificant modification to the absorption properties of the coating (Supporting Information, Figure SI(2)), and moreover surfactants were mostly removed after the postcoating treatments.

For the coating of acrylic and PDMS backing, we employed SDS (sodium dodecyl sulfate)-stabilized SWNT aqueous solution. An aqueous solution is used to avoid swelling of the chosen polymer matrix by common organic solvents. An appropriate amount of SWNTs were sonicated with 5 mL of 0.5 wt % SDS−water solution for 5 min prior to centrifuge coating. Centrifuge coating was carried out at 75 °C with a rotational speed of 5000 rpm (a_c = 91 g) for 45 min. The coated electrodes were rinsed in distilled water with no further acid treatment. Coatings obtained on PDMS were not very homogeneous due to the highly hydrophobic nature of PDMS. We suggest that precoating surface plasma treatment should improve the wetting. It was also found that the electrical-optical performance of the elastomer-backed electrodes is much poorer than the same nonacid treated SWNT on PET (Table c in Supporting Information, Figure SI(2). This is probably because the particles have been partially embedded in the soft substrate due to the centrifuge action.

Electrode Testing. To ensure consistency and reproducibility, all the experimental techniques were preliminarily checked with an ITO-coated PET reference. The ITO-coated-PET film was purchased from Sigma Aldrich, with a nominal ITO thickness of 75 nm and quoted sheet resistance of 70−100 Ω/m^2. The PET backing layer for this ITO is ∼0.1 mm. Sheet resistance was determined using Lucas/Signatone 4-probe station (4-probe head SP4-40045TFY) connected to a voltage source, a current meter (Agilent Digital multimeter) and a voltage meter (Keithley 6512). Absorption spectrum was collected using CARY 300Bio UV−vis spectrometer (model EL02035941). The coated substrates were attached to one side of a cuvette and inserted into the measuring slot for spectrum collection. The net absorption of the SWNT-coating was subsequently calculated by subtracting the absorption due to the pure substrate layer on the cuvette reference. For the static and cyclic bending test, resistance of a known length of coating was monitored using the Agilent digital multimeter.

Acknowledgment. We thank J. Blundell, Y. Ji, S. Mahajan, T. Knowles, A. Buell, and C. Chimerel for many helpful discussions and technical assistance. We are also grateful for the financial support from the Gates Cambridge Trust and St John's College Benefactor Scholarship.

Supporting Information Available: Centrifuge coating procedures and principles with Figure SI(1), the model validation including Figures SI(2)−SI(4). This material is available free of charge *via* the Internet at http://pubs.acs.org.

REFERENCES AND NOTES

1. Artukovic, E.; Kaempgen, M.; Hecht, D. S.; Roth, S.; Gruner, G. Transparent and Flexible Carbon Nanotube Transistors. *Nano Lett.* **2005,** *5*, 757–760.
2. Zhang, D. H.; Ryu, K.; Liu, X. L.; Polikarpov, E.; Ly, J.; Tompson, M. E.; Zhou, C. W. Transparent, Conductive, and Flexible Carbon Nanotube Films and Their Application in Organic Light-Emitting Diodes. *Nano Lett.* **2006,** *6*, 1880–1886.
3. Yoon, Y. H.; Song, J. W.; Kim, D.; Kim, J.; Park, J. K.; Oh, S. K.; Han, C. S. Transparent Film Heater Using Single-Walled Carbon Nanotubes. *Adv. Mater.* **2007,** *19*, 4284–4287.
4. Iijima, S.; Ichinashi, T. Single-Shell Carbon Nanotubes of 1-nm Diameter. *Nature* **1993,** *363*, 603–605.
5. Geim, A. K.; Novoselov, K. S. The Rise of Graphene. *Nat. Mater.* **2007,** *6*, 183.
6. Wu, Z. C.; Chen, Z. H.; Du, X.; Logan, J. M.; Sippel, J.; Nikolou, M.; Kamaras, K.; Reynolds, J. R.; Tanner, D. B.; Hebard, A. F.; *et al*. Transparent, Conductive Carbon Nanotube Films. *Sicence* **2004,** *305*, 1273–1276.
7. Eda, G.; Fanchini, G.; Chhowalla, M. Large-Area Ultrathin Films of Reduced Graphene Oxide as a Transparent and Flexible Electronic Material. *Nat. Nanotechnol.* **2008,** *3*, 270–274.
8. Kim, K. S.; Zhao, Y.; Jang, H.; Lee, S. Y.; Kim, J. M.; Kim, K. S.; Ahn, J. H.; Kim, P.; Choi, J. Y.; Hong, B. H. Large-Scale Pattern Growth of Graphene Films for Stretchable Transparent Electrodes. *Nature* **2009,** *457*, 706–710.
9. Zhu, Y.; Murali, S.; Cai, W.; Li, X.; Suk, J. W.; Potts, J. R.; Ruoff, R. S. Graphene and Graphene Oxide: Synthesis, Properties, and Applications. *Adv. Mater.* **2010,** *22*, 3906–3924.
10. Bae, S.; Kim, H.; Lee, Y.; Xu, X. F.; Park, J. S.; Zheng, Y.; Balakrishnan, J.; Lei, T.; Kim, H. R.; Song, Y. I.; *et al*. Roll-to-Roll Production of 30-in. Graphene Films for Transparent Electrodes. *Nat. Nanotechnol.* **2010,** *5*, 574–578.
11. Geng, H. Z.; Kim, K. K.; So, K. P.; Lee, Y. S.; Chang, Y.; Lee, Y. H. Effect of Acid Treatment on Carbon Nanotube-Based Flexible Transparent Conducting Films. *J. Am. Chem. Soc.* **2007,** *129*, 7758–7759.
12. Li, Z. R.; Kandel, H. R.; Dervishi, E.; Saini, V.; Xu, Y.; Biris, A. R.; Lupu, D.; Salamo, G. J.; Biris, A. S. Comparative Study on Different Carbon Nanotube Materials in Terms of Transparent Conductive Coatings. *Langmuir* **2008,** *24*, 2655–2662.
13. De, S.; Higgins, T. M.; Lyons, P. E.; Doherty, E. M.; Nirmalraj, P. N.; Blau, W. J.; Boland, J. J.; Coleman, J. N. Silver Nanowire

Networks as Flexible, Transparent, Conducting Films: Extremely High DC to Optical Conductivity Ratios. *ACS Nano* **2009,** *3*, 1767–1774.
14. Scardaci, V.; Coull, R.; Coleman, J. N. Very Thin Transparent, Conductive Carbon Nanotube Films on Flexible Substrates. *Appl. Phys. Lett.* **2010,** *97*, 023114.
15. Becerril, H. A.; Mao, J.; Liu, Z.; Stoltenberg, R. M.; Bao, Z.; Chen, Y. Evaluation of Solution-Processed Reduced Graphene Oxide Films as Transparent Conductors. *ACS Nano* **2008,** *2*, 463–470.
16. Li, X. S.; Zhu, Y. W.; Cai, W. W.; Borysiak, M.; Han, B. Y.; Chen, D.; Piner, R. D.; Colombo, L.; Ruoff, R. S. Transfer of Large-Area Graphene Films for High-Performance Transparent Conductive Electrodes. *Nano Lett.* **2009,** *9*, 4359–4363.
17. Mattevi, C.; Eda, G.; Agnoli, S.; Miller, S.; Mkhoyan, K. A.; Celik, O.; Mostrogiovanni, D.; Granozzi, G.; Garfunkel, E.; Chhowalla, M. Evolution of Electrical, Chemical, and Structural Properties of Transparent and Conducting Chemically Derived Graphene Thin Films. *Adv. Funct. Mater.* **2009,** *19*, 2577–2583.
18. De, S.; King, P. J.; Lotya, M.; O'Neill, A.; Doherty, E. M.; Hernandez, Y.; Duesberg, G. S.; Coleman, J. N. Flexible, Transparent, Conducting Films of Randomly Stacked Graphene from Surfactant-Stabilized, Oxide-Free Graphene Dispersions. *Small* **2010,** *6*, 458–464.
19. Sreekumar, T.; Liu, T.; Kumar, S.; Ericson, L.; Hauge, R.; Smalley, R. Single-Wall Carbon Nanotube Films. *Chem. Mater.* **2003,** *15*, 175–178.
20. Meitl, M.; Zhou, Y.; Gaur, A.; Jeon, S.; Usrey, M.; Strano., M; Rogers, J. Solution Casting and Transfer Printing Single-Walled Carbon Nanotube Films. *Nano Lett.* **2004,** *4*, 1643–1647.
21. Armitage, N. P.; Gabriel, J.; Gruner, G. Quasi-Langmuir—Blodgett Thin Film Deposition of Carbon Nanotubes. *J. Appl. Phys.* **2004,** *95*, 3228–3230.
22. Hu, L; Hecht, D. S.; Gruner, G. Percolation in Transparent and Conducting Carbon Nanotube Networks. *Nano Lett.* **2004,** *4*, 2513–2517.
23. Tenent, R. C.; Barnes, T. M.; Bergeson, J. D.; Ferguson, A. J.; To, B; Gedvilas, L. M.; Heben, M. J.; Blackburn, J. L. Ultrasmooth, Large-Area, High-Uniformity, Conductive Transparent Single-Walled-Carbon-Nanotube Films for Photovoltaics Produced by Ultrasonic Spraying. *Adv. Mater.* **2009,** *21*, 3210–3216.
24. Doherty, E. M.; De, S.; Lyons, P. E.; Shmeliov, A.; Nirmalraj, P. N.; Scardaci, V.; Joimel, J.; Blau, W. J.; Boland, J. J. Coleman, J. N. The Spatial Uniformity and Electromechanical Stability of Transparent, Conductive Films of Single Walled Nanotubes. *Carbon* **2009,** *47*, 2466–2473.
25. Cai, W. W.; Zhu, Y. W.; Li, X. S.; Piner, R. D.; Ruoff, R. S. The Spatial Uniformity and Electromechanical Stability of Transparent, Conductive Films of Single Walled Nanotubes. *Appl. Phys. Lett.* **2009,** *95*, 123115.
26. Dressel, M.; Gruner; G. *Electrodynamics of Solids: Optical Properties of Electrons in Matter*: Cambridge University Press: Cambridge, U.K., 2002.
27. Doi, M.; Edwards, S. F. *The Theory of Polymer Dynamics*; Clarendon Press: Oxford, U.K., 1986.
28. Cairns, D. R.; Witte, R. P.; Sparacin, D. K.; Sachsman, S. M.; Paine, D. C.; Crawford, G. P.; Newton, R. R. Strain-Dependent Electrical Resistance of Tin-Doped Indium Oxide on Polymer Substrates. *Appl. Phys. Lett.* **2000,** *76*, 1425–1427.
29. Li, H.; Zhou, B.; Lin, Y.; Gu, L.; Wang, W.; Fernando, K. A. S.; Kumar, S.; Allard, L. F.; Sun, Y. P. Selective Interactions of Porphyrins with Semiconducting Single-Walled Carbon Nanotubes. *J. Am. Chem. Soc.* **2004,** *126*, 1014–1015.
30. Ji, Y.; Huang, Y. Y.; Tajbakhsh, A. R.; Terentjev, E. M. Polysiloxane Surfactants for the Dispersion of Carbon Nanotubes in Nonpolar Organic Solvents. *Langmuir* **2009,** *25*, 12325–12331.